



A high resolution wave propagation scheme for ideal Two-Fluid plasma equations

A. Hakim *, J. Loverich, U. Shumlak

Aerospace and Energetics Research Program, University of Washington, Seattle, WA 98195-2600, USA

Received 17 June 2005; received in revised form 24 February 2006; accepted 24 March 2006

Abstract

Algorithms for the solution of the five-moment ideal Two-Fluid equations are presented. The ideal Two-Fluid model is more general than the often used magnetohydrodynamic (MHD) model. The model takes into account electron inertia effects, charge separation and the full electromagnetic field equations and allows for separate electron and ion motion. The algorithm presented is the high resolution wave propagation method. The wave propagation method is based on solutions to the Riemann problem at cell interfaces. Operator splitting is used to incorporate the Lorentz and electromagnetic source terms. To preserve the divergence constraints on the electric and magnetic fields two different approaches are used. In the first approach Maxwell equations are rewritten in their mixed-potential form. In the second approach the so-called perfectly hyperbolic form of Maxwell equations are used which explicitly incorporate the divergence equations into the time stepping scheme. The algorithm is applied to a one-dimensional Riemann problem, ion-acoustic soliton propagation and magnetic reconnection. In each case Two-Fluid physics described by the ideal Two-Fluid model is highlighted.

© 2006 Elsevier Inc. All rights reserved.

Keywords: Plasma physics; Two-Fluid; High resolution; Gudonov method; Magnetic reconnection; Solitons; Maxwell equations

1. Introduction

A plasma is a gas that is significantly ionized, through heating or photo-ionization, and thus is composed of electrons, ions and neutrals. Plasmas are usually permeated by electromagnetic (EM) fields. In addition to long range smoothed or averaged EM fields there are localized short range micro-fields on individual particles. The long range fields act like body forces while the short range fields like collisions. The micro-fields are responsible for the transmission of pressure and viscous forces, for the conduction of particle energy, and for diffusion between components of the plasma [1]. The dynamical behavior of plasmas is also strongly dependent on frequency. At the lowest frequency the motion of the electrons and ions are locked together by electrostatic forces and the plasma behaves like an electrically conducting fluid. This is the regime of magnetohydrodynamics (MHD). At somewhat higher frequencies the electrons and ions can move relative

* Corresponding author.

E-mail address: ahakim@u.washington.edu (A. Hakim).

to each other, behaving like two separate, inter-penetrating fluids. At still higher frequencies the distribution function of the plasma species is driven by anisotropies in the velocity space. This regime is best described by the collisionless Boltzmann equation or Vlasov equation of kinetic theory.

In this paper numerical schemes are developed to simulate Two-Fluid plasma dynamics, i.e physics in the intermediate frequency regime between MHD and full kinetic theory. Due to the disparate scales on which plasma dynamics occurs a complete spectrum of mathematical models of plasmas can be derived. Among the most commonly used fluid models are the MHD model [2] and the Hall MHD model. In MHD the plasma is treated as a *single* electrically conducting fluid. Although in the Hall-MHD model a distinction is made between the bulk plasma velocity and electron velocity, electron inertia and displacement currents are ignored and electron and ion number-densities are assumed to be the same (quasi-neutrality). A more general approach, used in this paper, is to treat to the plasma as a mixture of multiple fluid species. In this *five-moment ideal Two-Fluid* model each plasma species is described by a set of fluid equations with electromagnetic body forces. The electromagnetic fields are modeled using Maxwell equations of electromagnetism. The Two-Fluid model retains both electron inertia effects and the displacement currents and also allows for ion and electron demagnetization.

In this paper, and in [3], an attempt is made to develop general purpose algorithms for the solution of the ideal full Two-Fluid equations. Applications presented here also show that Two-Fluid effects are important in many plasma regimes and hence must be taken into account to get a proper description of the physics.

The rest of this paper is organized as follows. First, some aspects of ideal Two-Fluid physics are described. Length scales at which Two-Fluid effects become important are then derived. Often the divergence constraints in Maxwell equations are not considered in numerical algorithms. To obtain correct solutions for initial-boundary value problems numerical schemes must incorporate the divergence constraints explicitly. Here two different approaches are adopted: a mixed potential formulation of Maxwell equations and the so-called perfectly hyperbolic Maxwell equations [4]. Next a high-resolution wave propagation scheme [5] for the solution of these equations is presented. This scheme, originally developed by Randall LeVeque, has been extensively used to study fluid dynamics, elasticity, MHD [6], etc. Although a similar scheme was used for the one-dimensional Two-Fluid Riemann problem [7], the application of this scheme to multi-dimensional ideal Two-Fluid system is first in the literature. A number of applications of the algorithm are then presented. In one dimension a Riemann problem and strongly nonlinear soliton propagation are studied. In two dimensions magnetic reconnection is studied. It is shown that the reconnection flux from the Two-Fluid model agrees well with that computed from full particle and hybrid simulations.

2. Two-Fluid physics

In collisionless plasmas collective interactions dominate the plasma dynamics. In this case a general description of the plasma is given by the Vlasov–Maxwell equations [8]. These describe the temporal evolution of a particle distribution function in a six-dimensional spatial and velocity space. The distribution function evolves under the influence of electromagnetic forces which are in turn determined by moments of the distribution function taken over velocity space. As the distribution function evolves in a seven-dimensional space numerical solutions of the Vlasov–Maxwell equations for realistic length and time scales are not computationally feasible. To reduce the number of independent variables fluid approximations are derived by taking moments of the Vlasov equation over velocity space. Assuming no heat flow and a scalar fluid pressure the following *five-moment ideal Two-Fluid equations* listed below are obtained for each species in the plasma

$$\frac{\partial n}{\partial t} + \frac{\partial}{\partial x_j}(nu_j) = 0, \quad (1)$$

$$m \frac{\partial}{\partial t}(nu_k) + \frac{\partial}{\partial x_j}(p\delta_{kj} + mnu_k u_j) = nq(E_k + \epsilon_{kij}u_i B_j), \quad (2)$$

$$\frac{\partial \mathcal{E}}{\partial t} + \frac{\partial}{\partial x_j}(u_j p + u_j \mathcal{E}) = qnu_j E_j. \quad (3)$$

Here n is the number density, \mathbf{u} is the mean fluid velocity, p is the fluid scalar pressure and \mathcal{E} is the fluid total energy given by

$$\mathcal{E} = \frac{p}{\gamma - 1} + \frac{1}{2} m n u_i u_i, \quad (4)$$

where $\gamma = 5/3$ is the adiabatic index. Further \mathbf{E} is the electric field, \mathbf{B} is the magnetic flux density, q and m are the charge and mass of the plasma species and ϵ_{kmj} is the completely anti-symmetric Cevi–Levita pseudo-tensor which is defined to be ± 1 for even/odd permutations of (1,2,3) and zero otherwise. Summation over repeated indices is assumed. The electromagnetic fields appearing in the source terms of the fluid equations are determined using Maxwell equations [9]

$$\nabla \times \mathbf{E} = -\frac{\partial \mathbf{B}}{\partial t}, \quad (5)$$

$$\nabla \times \mathbf{B} = \mu_0 \mathbf{J} + \frac{1}{c^2} \frac{\partial \mathbf{E}}{\partial t}, \quad (6)$$

$$\nabla \cdot \mathbf{E} = \frac{\varrho_c}{\epsilon_0}, \quad (7)$$

$$\nabla \cdot \mathbf{B} = 0. \quad (8)$$

Here μ_0 and ϵ_0 are the permeability and permittivity of free space, $c = (\mu_0 \epsilon_0)^{-1/2}$ is the speed of light and, ϱ_c and \mathbf{J} are the charge density and the current density defined by

$$\varrho_c \equiv \sum qn, \quad (9)$$

$$\mathbf{J} \equiv \sum qn\mathbf{u}. \quad (10)$$

The summations in Eqs. (9) and (10) are over all species present in the plasma. For a plasma with s species there are $5s + 8$ equations in the system.

The ideal Two-Fluid model is more general than the MHD or the Hall-MHD models. To derive conditions under which Two-Fluid effects, not included in the MHD or Hall MHD model, are important, scalar and vector potentials, ϕ , \mathbf{A} are introduced. In terms of these the electric and magnetic fields are expressed as

$$\mathbf{E} = -\nabla\phi + \partial\mathbf{A}/\partial t, \quad (11)$$

$$\mathbf{B} = \nabla \times \mathbf{A}. \quad (12)$$

Next, defining a *generalized momentum*, $\mathbf{P} \equiv m\mathbf{u} + q\mathbf{A}$ and a *generalized vorticity*, $\mathbf{\Omega} \equiv \nabla \times \mathbf{P} = m\boldsymbol{\omega} + q\mathbf{B}$, where $\boldsymbol{\omega} = \nabla \times \mathbf{u}$ is the fluid vorticity, the non-conservative form of the momentum equation is written as

$$\frac{\partial \mathbf{P}}{\partial t} - \mathbf{u} \times \mathbf{\Omega} = -\frac{\nabla p}{n} + \nabla(mu^2/2 + \phi), \quad (13)$$

which is a balance law for the generalized momentum [10]. Taking the curl of Eq. (13) gives

$$\frac{\partial \mathbf{\Omega}}{\partial t} - \nabla \times (\mathbf{u} \times \mathbf{\Omega}) = -\nabla \times (\nabla p/n). \quad (14)$$

This equation applies to each species in the plasma and, for example, for a hydrogen plasma there are two such equations. Eq. (14) can be compared to the ideal MHD result

$$\frac{\partial \mathbf{B}}{\partial t} - \nabla \times (\mathbf{v} \times \mathbf{B}) = 0, \quad (15)$$

where \mathbf{v} is the “bulk” or MHD single-fluid velocity, the Hall-MHD result [11]

$$\frac{\partial \mathbf{B}}{\partial t} - \nabla \times (\mathbf{u}_e \times \mathbf{B}) = -\nabla \times (\nabla p_e/en), \quad (16)$$

where e is electron charge, and the Euler (neutral) fluid result

$$\frac{\partial \boldsymbol{\omega}}{\partial t} - \nabla \times (\mathbf{v} \times \boldsymbol{\omega}) = -\nabla \times (\nabla p/\rho), \quad (17)$$

where ρ is the mass density. From these equations it is clear that the Two-Fluid equations span the complete range from neutral fluids, to Hall-MHD to MHD: $\mathbf{B} \rightarrow \mathbf{0}$ corresponds to neutral fluid limit, $m_e/m_i \rightarrow 0$

Table 1
Typical density, temperature and magnetic field strength of plasmas in various environments

Plasma	ne (m ⁻³)	T (K)	B (T)	λ_D (m)	ω_p (s ⁻¹)	ω_c (s ⁻¹)	r_L (m)	l (m)
Tokamak	10^{20}	10^8	10	10^{-4}	10^{12}	10^{12}	10^{-5}	10^{-4}
Ionosphere	10^{12}	10^3	10^{-5}	10^{-3}	10^8	10^6	10^{-1}	1
Magnetosphere	10^7	10^7	10^{-8}	10^2	10^5	10^3	10^4	10^3
Solar core	10^{32}	10^7	–	10^{-11}	10^{18}	–	–	10^{-10}
Solar wind	10^6	10^5	10^{-9}	10	10^5	10^2	10^4	10^3

The various plasma parameters and their meanings are defined in the text.

corresponds to Hall-MHD while $\omega/(qB/m) \rightarrow 0$, which, as shown below, is the same as vanishing electron and ion-skin depths or Larmor radii correspond to ideal MHD limit.

Examining the generalized vorticity $\mathbf{\Omega} = m(\boldsymbol{\omega} + q\mathbf{B}/m)$ it is clear that for Two-Fluid effects to be important

$$\omega/\omega_c \geq \mathcal{O}(1), \quad (18)$$

where $\omega_c \equiv qB/m$ is the cyclotron frequency. Using the fluid thermal velocity $u_T \equiv \sqrt{2p/(mn)}$ as a reference speed and some reference length L , $\omega \approx u_T/L$ and hence the condition

$$u_T/(L\omega_c) = r_L/L \geq \mathcal{O}(1), \quad (19)$$

where $r_L \equiv u_T/\omega_c$ is defined as the Larmor radius, is obtained. Instead of the fluid thermal velocity if the typical speed is assumed to be the Alfvén speed,¹ $u_A \equiv B/\sqrt{\mu_0 mn}$, then the condition

$$u_A/(L\omega_c) = (c/\omega_p)/L \geq \mathcal{O}(1), \quad (20)$$

where $\omega_p \equiv \sqrt{nq^2/\epsilon_0 m}$ is the plasma frequency, is obtained. It should be emphasized that the plasma frequency, Larmor radii and cyclotron frequency are each defined separately for each plasma species.

In summary, Two-Fluid effects are important when, for both ions and electrons, $r_L/L \geq \mathcal{O}(1)$ and/or when $l/L \geq \mathcal{O}(1)$, where $l \equiv c/\omega_p$ is the skin depth. Conversely, in the limit in which the length scales are much larger than the electron-skin depth, but smaller than the ion-skin depth, Hall-MHD is an adequate model, while in the limit in which the scale lengths are larger than ion-skin depths the MHD description is adequate.

Table 1 lists order of magnitude values of density, temperature and magnetic field strength for various plasma environments. Using these the values of the Deby length (which determines the length scale over which non-neutral effects are important), the ion plasma and cyclotron frequency, and the ion Larmor radius and skin depths are listed. From the table it is clear that for space plasma applications the Larmor radii and skin depths are large and hence Two-Fluid effects are important for these applications. Further, not shown in this table, compact fusion devices like field-reversed configurations [12] have plasma skin-depths comparable to the device dimensions. Hence, Two-Fluid effects are important to understand the complete physics, specially anomalous resistivity arising from Two-Fluid micro-instabilities [13,14].

3. Nature of Two-Fluid source terms

Many partial differential equations are classified as either *elliptic*, *parabolic* or *hyperbolic*. The five-moment ideal Two-Fluid equations have hyperbolic homogeneous parts. This means, crudely, that disturbances at some spatially location cause changes in the dynamics at some other location after some finite time interval. The disturbances travel as waves and hence wave propagation plays an essential role in the solution of hyperbolic equations. However, the presence of source terms in the Two-Fluid models significantly affects the dynamics. In this section the source terms of the ideal Two-Fluid equations are examined for a plasma with one electron and one ion species. It is shown that the source terms are non-dissipative and have undamped oscillating solutions. The nature of the source terms puts restrictions on the numerical methods that can be used and these are discussed later in this section.

¹ This can happen when there is an equipartition between the kinetic, $mmu^2/2$, and electromagnetic energy $B^2/(2\mu_0) + \epsilon_0 E^2/2 \approx B^2/(2\mu_0)$.

Not all equations in the Two-Fluid system have sources. Collecting the terms that have sources and assuming that the advection terms vanish (i.e. all spatial derivatives vanish) the following ordinary differential equation

$$\frac{d\mathbf{q}}{dt} = \mathbf{s} \quad (21)$$

is obtained, where $\mathbf{q} = [u_e, v_e, w_e, u_i, v_i, w_i, E_x, E_y, E_z]$ and

$$\mathbf{s} = \begin{bmatrix} r_e(E_x + v_e B_z - w_e B_y) \\ r_e(E_y + w_e B_x - u_e B_z) \\ r_e(E_z + u_e B_y - v_e B_x) \\ r_i(E_x + v_i B_z - w_i B_y) \\ r_i(E_y + w_i B_x - u_i B_z) \\ r_i(E_z + u_i B_y - v_i B_x) \\ -(r_e \rho_e u_e + r_i \rho_i u_i) / \epsilon_0 \\ -(r_e \rho_e v_e + r_i \rho_i v_i) / \epsilon_0 \\ -(r_e \rho_e w_e + r_i \rho_i w_i) / \epsilon_0 \end{bmatrix}. \quad (22)$$

Here the subscripts $\alpha = \{e, i\}$ stand for electron and ion variables, $r_\alpha \equiv q_\alpha / m_\alpha$ and $u_\alpha, v_\alpha, w_\alpha$ represent the components of the velocity vector. The energy equations are not included in the analysis as energy does not appear in the source terms explicitly.

From Eq. (21) it is clear that \mathbf{s} is linear in \mathbf{q} and hence the solutions of Eq. (21) are classified by examining the eigenvalues of the Jacobian $\mathbf{J} \equiv \partial \mathbf{s} / \partial \mathbf{q}$. It can be proved that the non-zero eigenvalues of \mathbf{J} are all purely imaginary. Defining the plasma frequency, $\omega_{p\alpha}$, and cyclotron frequency, $\omega_{c\alpha}$, by

$$\omega_{p\alpha} = \sqrt{n_\alpha q_\alpha^2 / \epsilon_0 m_\alpha}, \quad (23)$$

$$\omega_{c\alpha} = q_\alpha B / m_\alpha, \quad (24)$$

the first three eigenvalues of \mathbf{J} are $0, \pm i\omega_p$, where $\omega_p^2 = \omega_{pe}^2 + \omega_{pi}^2$ and $i = \sqrt{-1}$. The other six eigenvalues are the roots of a sixth order polynomial with imaginary roots.

The above analysis shows that the source terms of the Two-Fluid model are not dissipative but describe undamped oscillations. In contrast, in most commonly studied hyperbolic balance laws, specially relaxation systems, the eigenvalues of the source Jacobian are real and negative. Thus such relaxation systems can describe decaying solutions in certain physical situations. In the ideal Two-Fluid model, however, the source terms do not add any dissipation to the system. This has some important implications for the numerical methods that can be used for the solution of the full (with advection term) system. First, low order explicit time stepping schemes cannot be used as these are unstable to the oscillation equations. Second, if the physics is to be resolved then several time steps must be taken per oscillation. Thus implicit methods do not have any advantage over explicit methods as small time steps must be taken to resolve complete physics in any case. Further, although an implicit scheme is stable with larger time steps it is dissipative for the oscillation equation. Hence flow features get smeared out, specially at or near equilibrium. Finally, in the f-wave approach of LeVeque described further on the source terms cannot be directly incorporated in the Riemann solver (see Eq. (61)) as the resulting scheme is unstable.

4. Divergence constraints in Maxwell equations

At first sight Maxwell equations, Eqs. (5)–(8), seem to be overdetermined: there are eight equations for the six field components \mathbf{E} and \mathbf{B} . It is commonly believed that the divergence equations, Eqs. (7) and (8), are simply constraints and if initially satisfied only the curl equations are sufficient to evolve the EM fields correctly. Thus, often the divergence equations are simply ignored in numerical electromagnetics. However, this is strictly true only for initial value problems, i.e. for problems on an infinite domain. As Jiang et al. [15] have

shown for initial-boundary value problems Maxwell equation are in fact not overdetermined and the divergence equations need to be explicitly included in the solution. Even for numerical solution to initial value problems, the evolving numerical fields may not satisfy the divergence equations and hence spurious solutions may be obtained. In this paper two different approaches, described below, are used to take the divergence equations into account.

The first approach is to introduce a scalar potential, ϕ , and a vector potential, \mathbf{A} , in terms of which the EM fields are calculated as

$$\mathbf{E} = -\nabla\phi + \partial\mathbf{A}/\partial t, \quad (25)$$

$$\mathbf{B} = \nabla \times \mathbf{A}. \quad (26)$$

Introducing these expressions in Maxwell equations it can be shown that the potentials satisfy inhomogeneous wave equations

$$\nabla^2\phi - \frac{1}{c^2} \frac{\partial^2\phi}{\partial t^2} = \frac{\rho_c}{\epsilon_0}, \quad (27)$$

$$\nabla^2\mathbf{A} - \frac{1}{c^2} \frac{\partial^2\mathbf{A}}{\partial t^2} = -\mu_0\mathbf{J}. \quad (28)$$

In deriving these equation the *Lorentz gauge condition*

$$\nabla \cdot \mathbf{A} = -\frac{1}{c^2} \frac{\partial\phi}{\partial t} \quad (29)$$

is used. Another gauge that can be used is the *Coulomb gauge*, $\nabla \cdot \mathbf{A} = 0$. With this the equation for the scalar potential reduces to a Poisson equation. The main disadvantage of the Coulomb gauge over the Lorentz gauge is that now an elliptic equation needs to be solved in addition to the hyperbolic fluid equations which is not convenient for numerical solution. The mixed potential equations are now used instead of Maxwell equations to advance the EM fields. The inhomogeneous wave equations can be rewritten as a system of first order equations. In this way a solver for second order equations is avoided. However, the disadvantage of this approach is that in three dimensions the two second order equations give 16 first order equations, thus increasing computation time. Further, the Lorentz gauge condition needs to be enforced. However, a peculiar feature of the gauge condition is that the derivatives appearing in it do not appear in the computation of the EM fields. Thus it might be simpler to apply a “gauge cleaning” procedure at each step. The simulations performed with this model show that the gauge condition usually is satisfied to within numerical precision and no such cleaning is needed.

The second approach is to modify Maxwell equations by adding two more field variables to take into account the two divergence equations. In fact, by introducing two extra variables, Jiang et al. [15] were able to prove that Maxwell equations are not overdetermined. However, these authors then went on to derive second order, so-called “curl–curl”, equations in which these extra variables do not appear. An attractive feature of adding more variables is that modified equations of hyperbolic type can be obtained, in contrast to the mixed hyperbolic/elliptic type of the original equations. These *perfectly hyperbolic Maxwell equations* (PHM) read [4,16,17]

$$\frac{\partial\mathbf{B}}{\partial t} + \nabla \times \mathbf{E} + \gamma\nabla\psi = 0, \quad (30)$$

$$\epsilon_0\mu_0 \frac{\partial\mathbf{E}}{\partial t} - \nabla \times \mathbf{B} + \chi\nabla\phi = -\mu_0\mathbf{J}, \quad (31)$$

$$\frac{1}{\chi} \frac{\partial\phi}{\partial t} + \nabla \cdot \mathbf{E} = \frac{\rho_c}{\epsilon_0}, \quad (32)$$

$$\frac{\epsilon_0\mu_0}{\gamma} \frac{\partial\psi}{\partial t} + \nabla \cdot \mathbf{B} = 0. \quad (33)$$

Here ψ and ϕ are “correction potentials” and γ and χ are error propagation speeds. As $\gamma, \chi \rightarrow \infty$ the divergence constraints are satisfied exactly. Thus more accurate solutions can be obtained with large values of these

speeds, however at the expense of larger computational time. Usually $\gamma, \chi = c$ or $2c$ gives a good compromise between accuracy and speed. Thus, unlike the mixed-potential formulation the PHM formulation preserve the divergence constraints only approximately.

A number of simulations were performed to compare the mixed potential and PHM equations approaches. It was observed that both mixed-potential and PHM approaches could satisfy the divergence equations to second-order accuracy as needed by the wave propagation scheme described below. In the results presented the PHM model is used for all simulations.

5. High resolution wave propagation scheme

Inhomogeneous partial differential equations with hyperbolic homogeneous parts are called *balance laws* and arise in a large number of physical applications. Balance laws are put in the generic divergence form

$$\frac{\partial \mathbf{q}}{\partial t} + \nabla \cdot \mathbf{f} = \mathbf{s}, \quad (34)$$

where \mathbf{q} represents the conserved variables, \mathbf{f} the fluxes and \mathbf{s} the source terms. For m balance laws in d spatial dimensions $\mathbf{q}, \mathbf{s} \in \mathbb{R}^m$ and $\mathbf{f} \in \mathbb{R}^{m \times d}$. A conservation law is said to have a hyperbolic homogeneous part if for all unit vectors $\boldsymbol{\omega} \in \mathbb{R}^d$ the flux Jacobian, $\mathbf{A} \in \mathbb{R}^{m \times m}$, defined by

$$\mathbf{A} \equiv \frac{\partial(\mathbf{f} \cdot \boldsymbol{\omega})}{\partial \mathbf{q}} \quad (35)$$

has real eigenvalues and a complete set of right eigenvectors [5,18]. If, further, the eigenvalues are all distinct the homogeneous part is called *strictly hyperbolic*. It can be shown that the five-moment ideal Two-Fluid equations have hyperbolic homogeneous parts. It can also be shown that higher-moment approximations to the Vlasov equations are also hyperbolic. Hence the high resolution wave propagation method, briefly described below, can be directly applied to such equations. For a complete description of this method, see [5,19,20].

5.1. First order scheme

In two dimensions a homogeneous hyperbolic equation is written as

$$\frac{\partial \mathbf{q}}{\partial t} + \frac{\partial \mathbf{f}_1}{\partial x} + \frac{\partial \mathbf{f}_2}{\partial y} = 0, \quad (36)$$

where \mathbf{f}_1 and \mathbf{f}_2 are the fluxes in the X and Y direction, respectively. This equation is discretized on a rectangular domain $\Omega \in [x_a, x_b] \times [y_a, y_b]$ by introducing cells $I_{ij} = [x_{i-1/2}, x_{i+1/2}] \times [y_{j-1/2}, y_{j+1/2}]$, where $x_{i-1/2}$ and $y_{j-1/2}$ are coordinates along cell edges and (x_i, y_i) , where $x_i \equiv (x_{i-1/2} + x_{i+1/2})/2$ and $y_j \equiv (y_{j-1/2} + y_{j+1/2})/2$, are the coordinates of the cell center. Integrating the conservation law equation (36) over cell I_{ij} and from time t_n to t_{n+1} the update formula

$$Q_{ij}^{n+1} = Q_{ij}^n - \frac{\Delta t}{\Delta x} \left([\mathcal{F}_1]_{i+1/2,j}^{n+1/2} - [\mathcal{F}_1]_{i-1/2,j}^{n+1/2} \right) - \frac{\Delta t}{\Delta y} \left([\mathcal{F}_2]_{i,j+1/2}^{n+1/2} - [\mathcal{F}_2]_{i,j-1/2}^{n+1/2} \right) \quad (37)$$

is obtained. In this expression Q_{ij}^n represents the cell average

$$Q_{ij}^n \approx \frac{1}{\Delta x \Delta y} \int_{y_{j-1/2}}^{y_{j+1/2}} \int_{x_{i-1/2}}^{x_{i+1/2}} \mathbf{q}(x, y, t) \, dx \, dy, \quad (38)$$

$\Delta x \equiv x_{i+1/2} - x_{i-1/2}$, $\Delta y \equiv y_{j+1/2} - y_{j-1/2}$, $\Delta t \equiv t_{n+1} - t_n$ and $[\mathcal{F}_{1,2}]$ are numerical fluxes at the cell interfaces defined as

$$[\mathcal{F}_1]_{i-1/2,j}^{n+1/2} \approx \frac{1}{\Delta t} \int_{t_n}^{t_{n+1}} \mathbf{f}_1(q(x_{i-1/2}, y_j, t), x_{i-1/2}, y_j) \, dt, \quad (39)$$

$$[\mathcal{F}_2]_{i,j-1/2}^{n+1/2} \approx \frac{1}{\Delta t} \int_{t_n}^{t_{n+1}} \mathbf{f}_2(q(x_i, y_{j-1/2}, t), x_i, y_{j-1/2}) \, dt. \quad (40)$$

Eq. (37) is a general update formula for finite volume schemes and several different methods can be constructed by selecting various approximations for the numerical fluxes. In this paper a specific finite volume method, the *high-resolution wave propagation method*, introduced by LeVeque is used. To introduce this method it should be first noted that at a given cell interface the value of the cell averages in the cells sharing that edge will be, in general, discontinuous. This suggests that the numerical flux at the cell edge be determined by solving a Riemann problem at that edge.

The Riemann problem is an initial value problem

$$\frac{\partial \mathbf{q}}{\partial t} + \frac{\partial \mathbf{f}_1}{\partial x} = 0, \quad x \in \mathbb{R} \quad (41)$$

with initial conditions $\mathbf{q}(x < 0, 0) = \mathbf{q}_l$ and $\mathbf{q}(x > 0, 0) = \mathbf{q}_r$, where $\mathbf{q}_{l,r}$ are constant vectors. For linear hyperbolic systems the Riemann problem has exact solutions. For nonlinear problems a linearization is introduced to obtain solutions valid around $x = 0$ for short times interval. Assuming that Eq. (41) is a linear hyperbolic equation it is written as

$$\frac{\partial \mathbf{q}}{\partial t} + \mathbf{A}_1 \frac{\partial \mathbf{q}}{\partial x} = 0, \quad (42)$$

where \mathbf{A}_1 is the flux Jacobian and is constant for the assumed linear system. Let l^p , r^p and s^p be the left eigenvectors, right eigenvectors and eigenvalues of \mathbf{A}_1 . As the system is hyperbolic the eigenvalues must be all real and the eigenvectors are assumed to be orthonormal. Multiplying by the left eigenvector l^p a system of uncoupled wave equations

$$\frac{\partial w^p}{\partial t} + s^p \frac{\partial w^p}{\partial x} = 0 \quad (43)$$

is obtained, where $w^p \equiv l^p \cdot \mathbf{q}$. This has solutions $w^p(x, t) = w_0^p(x - s^p t)$, where $w_0(x) = l^p \cdot \mathbf{q}(x, 0)$. Once $w^p(x, t)$ is determined $\mathbf{q}(x, t) = \sum_p w^p r^p$ and hence the Riemann problem for linear systems (or linearized systems) is solved exactly.

In the wave propagation method the solution to the Riemann problem at each cell interface is used to derive the following approximation to the numerical fluxes

$$[\mathcal{F}_1]_{i-1/2,j} = \frac{1}{2} \left([\mathbf{f}_1]_{i,j} + [\mathbf{f}_1]_{i-1,j} \right) - \frac{1}{2} \left(\mathcal{A}_1^+ \Delta Q_{i-1/2,j} - \mathcal{A}_1^- \Delta Q_{i-1/2,j} \right). \quad (44)$$

Introducing this expression in the update formula along with an analogous expression for the Y direction numerical flux gives

$$Q_{ij}^{n+1} = Q_{ij}^n - \frac{\Delta t}{\Delta x} \left[\mathcal{A}_1^+ \Delta Q_{i-1/2,j} + \mathcal{A}_1^- \Delta Q_{i+1/2,j} \right] - \frac{\Delta t}{\Delta y} \left[\mathcal{A}_2^+ \Delta Q_{i,j-1/2} + \mathcal{A}_2^- \Delta Q_{i,j+1/2} \right]. \quad (45)$$

In these expressions the *fluctuations* $\mathcal{A}_1^\pm \Delta Q_{i-1/2}$ (dropping the j subscript) stand for

$$\mathcal{A}_1^- \Delta Q_{i-1/2} = \sum_{p:s_{i-1/2}^p < 0} \mathcal{Z}_{i-1/2}^p + \frac{1}{2} \mathbb{Z}_{i-1/2}, \quad (46)$$

$$\mathcal{A}_1^+ \Delta Q_{i-1/2} = \sum_{p:s_{i-1/2}^p > 0} \mathcal{Z}_{i-1/2}^p + \frac{1}{2} \mathbb{Z}_{i-1/2}, \quad (47)$$

where

$$\mathcal{Z}_{i-1/2}^p = l_{i-1/2}^p \cdot \left([\mathbf{f}_1]_i - [\mathbf{f}_1]_{i-1} \right) r_{i-1/2}^p \quad (48)$$

and

$$\mathbb{Z}_{i-1/2} = \sum_{p:s_{i-1/2}^p = 0} \mathcal{Z}_{i-1/2}^p. \quad (49)$$

In deriving Eq. (45) the identity

$$\mathcal{A}_1^- \Delta Q_{i-1/2} + \mathcal{A}_1^+ \Delta Q_{i-1/2} = \sum_p \mathcal{Z}_{i-1/2}^p = [\mathbf{f}_1]_i - [\mathbf{f}_1]_{i-1} \quad (50)$$

which follows from the definition of $\mathcal{Z}_{i-1/2}^p$ (see Eq. (48)) is used. The eigenvectors $r_{i-1/2}^p$, $l_{i-1/2}^p$ and the eigenvalues $s_{i-1/2}^p$ needed in these expressions are computed using the flux Jacobian at the cell interfaces. For linear system this eigensystem is constant and does not depend on the solution. For nonlinear systems an appropriate averaging must be used before determining the eigensystem. In the simulations presented here *Roe averages* [21] are used for the Euler equations. Unlike conventional Godunov schemes the wave propagation method presented above can also be applied directly to situations in which the fluxes explicitly depend on spatial coordinates. Further, it is not necessary that Roe averages be used (or even exist) for the hyperbolic system being solved: simple arithmetic averages are usually sufficient. It can be shown that even when Roe averages are not available the scheme continues to be conservative [19]. Further, if Roe averages are used (or the system is linear) it can be shown that the zero wave, $\mathbb{Z}_{i-1/2}$, vanishes.

5.2. High resolution corrections

The scheme equation (45) is only first order accurate. To achieve second order accuracy high resolution corrections are added. These corrections are derived by taking into account second order terms in a Taylor series expansion of the conserved variables. The scheme equation (45) is modified to read

$$\begin{aligned} Q_{ij}^{n+1} = Q_{ij}^n - \frac{\Delta t}{\Delta x} \left[\mathcal{A}_1^+ \Delta Q_{i-1/2,j} + \mathcal{A}_1^- \Delta Q_{i+1/2,j} \right] - \frac{\Delta t}{\Delta y} \left[\mathcal{A}_2^+ \Delta Q_{i,j-1/2} + \mathcal{A}_2^- \Delta Q_{i,j+1/2} \right] \\ - \frac{\Delta t}{\Delta x} \left([\tilde{\mathcal{F}}_1]_{i+1/2,j} - [\tilde{\mathcal{F}}_1]_{i-1/2,j} \right) - \frac{\Delta t}{\Delta y} \left([\tilde{\mathcal{F}}_2]_{i,j+1/2} - [\tilde{\mathcal{F}}_2]_{i,j-1/2} \right), \end{aligned} \quad (51)$$

where $[\tilde{\mathcal{F}}_1]_{i-1/2}$ (dropping the j subscript) is a *correction flux* given by

$$[\tilde{\mathcal{F}}_1]_{i-1/2} = \frac{1}{2} \sum_p \text{sign}(s_{i-1/2}^p) \left(1 - \frac{\Delta t}{\Delta x} |s_{i-1/2}^p| \right) \mathcal{Z}_{i-1/2}^p. \quad (52)$$

With this correction the high resolution wave propagation method is equivalent to the standard Lax–Wendroff method. Although the scheme equation (51) is second order accurate spurious oscillations can occur at or near discontinuities. The scheme can be limited to reduce the formal accuracy to first order at discontinuities by replacing $\mathcal{Z}_{i-1/2}^p$ Eq. (52) by a *limited wave* $\tilde{\mathcal{Z}}_{i-1/2}^p = \mathcal{Z}_{i-1/2}^p \phi(\theta_{i-1/2}^p)$, where $\phi(\theta)$ is a suitable limiter function and

$$\theta_{i-1/2}^p \equiv \frac{\mathcal{Z}_{I-1/2}^p \cdot \mathcal{Z}_{i-1/2}^p}{\mathcal{Z}_{i-1/2}^p \cdot \mathcal{Z}_{i-1/2}^p} \quad (53)$$

with $I = i - 1$ if $s_{i-1/2}^p > 0$ and $I = i + 1$ if $s_{i-1/2}^p < 0$. For the results presented here the monotonized centered limiter, defined by,

$$\phi(\theta) = \max(0, \min((1 + \theta)/2, 2, 2\theta)) \quad (54)$$

is used. With the limiters the scheme is second order accurate in smooth regions when the flow is nearly aligned along one coordinate direction. At or near discontinuities the limiters reduce the scheme to first order accuracy. To make the scheme formally second order even when the flow is not aligned along a coordinate direction *transverse corrections*, discussed below, must be added.

5.3. Transverse corrections

In the first order and high resolution correction schemes waves are assumed to propagate normal to the cell interface. However, in multiple dimensions, due to the additional degrees of freedom, waves may also propagate in transverse directions. To take this into account *transverse corrections* are added to the update formula. The solution of the Riemann problem at cell edge $(i - 1/2, j)$ produces fluctuations traveling into

cells (i, j) and $(i - 1, j)$. For two-dimensional problems, however, these fluctuations should also affect the cells $(i - 1, j - 1)$, $(i - 1, j + 1)$, $(i, j + 1)$ and $(i, j - 1)$. To compute how these cells are affected first define left and right going fluctuations to which high resolution corrections have been added as

$$\mathcal{A}_1^\pm \Delta Q_{i-1/2}^* \equiv \mathcal{A}_1^\pm \Delta Q_{i-1/2} \mp \sum_p \text{sign}(s_{i-1/2}^p) \left(1 - \frac{\Delta t}{\Delta x} |s_{i-1/2}^p|\right) \tilde{\mathcal{L}}_{i-1/2}^p. \quad (55)$$

Next, to determine how much of each fluctuation travels in the transverse direction the fluctuations are decomposed using the flux Jacobian in the other coordinate direction. For example, the left and right going ($\pm X$ -direction) fluctuations are decomposed using the Y direction flux Jacobian and vice versa, i.e.

$$\mathcal{A}_1^\pm \Delta Q_{i-1/2,j}^* = \mathcal{A}_2^+ \mathcal{A}_1^\pm \Delta Q_{i-1/2,j}^* + \mathcal{A}_2^- \mathcal{A}_1^\pm \Delta Q_{i-1/2,j}^*. \quad (56)$$

Thus, for example, $\mathcal{A}_2^+ \mathcal{A}_1^+ \Delta Q_{i-1/2,j}^*$ indicates how much of the right going fluctuation is up going, while $\mathcal{A}_2^- \mathcal{A}_1^+ \Delta Q_{i-1/2,j}^*$ indicates how much of it is down going. Note that Eq. (56) is analogous to Eq. (50) which describes the splitting of the flux jump across an interface into fluctuations. As decomposition equation (56) again requires the eigenvalues, eigenvectors and, fluctuations it can be called a transverse Riemann solution. For three-dimensional problems further Riemann problems need to be solved to determine how much of the transverse waves travel in the third direction [20].

Once the transverse Riemann problem is solved the high resolution correction flux in Eq. (51) is replaced by

$$[\tilde{\mathcal{F}}_2]_{i,j+1/2} = [\tilde{\mathcal{F}}_2]_{i,j+1/2} - \frac{\Delta t}{2\Delta x} \mathcal{A}_2^+ \mathcal{A}_1^+ \Delta Q_{i-1/2,j}^*, \quad (57)$$

$$[\tilde{\mathcal{F}}_2]_{i,j-1/2} = [\tilde{\mathcal{F}}_2]_{i,j-1/2} - \frac{\Delta t}{2\Delta x} \mathcal{A}_2^- \mathcal{A}_1^+ \Delta Q_{i-1/2,j}^*, \quad (58)$$

$$[\tilde{\mathcal{F}}_2]_{i-1,j+1/2} = [\tilde{\mathcal{F}}_2]_{i-1,j+1/2} - \frac{\Delta t}{2\Delta x} \mathcal{A}_2^+ \mathcal{A}_1^- \Delta Q_{i-1/2,j}^*, \quad (59)$$

$$[\tilde{\mathcal{F}}_2]_{i-1,j-1/2} = [\tilde{\mathcal{F}}_2]_{i-1,j-1/2} - \frac{\Delta t}{2\Delta x} \mathcal{A}_2^- \mathcal{A}_1^- \Delta Q_{i-1/2,j}^*. \quad (60)$$

A similar method can be used to decompose the up and down going fluctuations into the right and left directions. The correction flux $[\tilde{\mathcal{F}}_1]_{i-1/2,j}$, for example, can then be modified in an analogous fashion as $[\tilde{\mathcal{F}}_2]_{i,j+1}$ shown above.

With the transverse terms included into the update formula the high resolution wave propagation method is formally second order in space and time for general smooth two-dimensional flow problems. It should be mentioned that even if the transverse terms are not used the scheme still gives second order accuracy. However, with the transverse terms the scheme is stable with Courant numbers upto one. Further the solution with and without the transverse terms can be significantly different in some situations. For example, in the reconnection simulation discussed in Section 7.3 if the transverse terms are not included “magnetic islands”, a numerical artifact, are observed. With the transverse terms such spurious solutions do not occur.

6. Handling source terms

In the high resolution wave propagation method the source terms are handled in two different ways. The first is to modify Eq. (48) to [19]

$$\mathcal{L}_{i-1/2} = l_{i-1/2}^p \cdot \left([\mathbf{f}_1]_i - [\mathbf{f}_1]_{i-1} - \Delta x [\mathbf{s}]_{i-1/2} \right) r_{i-1/2}^p, \quad (61)$$

where $[\mathbf{s}]_{i-1/2}$ is some average value of the source term calculated at the cell interface. Usually simple arithmetic averaging is sufficient. In this approach the source is directly taken into account while solving the Riemann problem. For solutions near or at equilibrium this is specially advantageous. However, this method suffers from two disadvantages. The first is that for two-dimensional balance laws the source must be split into two parts $\mathbf{s} = \mathbf{s}_1 + \mathbf{s}_2$ such that at equilibrium they satisfy

$$\frac{\partial \mathbf{f}_1}{\partial x} \approx \mathbf{s}_1, \quad (62)$$

$$\frac{\partial \mathbf{f}_2}{\partial y} \approx \mathbf{s}_2. \quad (63)$$

This may not be possible for all balance laws. However, for the Two-Fluid system with Maxwell equations replaced by mixed potentials such a splitting can be achieved although no such splitting exists with the PHM equations. The second disadvantage is specific to the source terms in the Two-Fluid equations. As the Two-Fluid source terms represent undamped oscillations explicit time stepping schemes are unstable. As the wave propagation method is an explicit single step method the scheme resulting from using Eq. (61) is observed to be unstable.

The other approach is to use operator splitting and solve the homogeneous system separately and incorporate the source term by solving the ordinary differential equation (ODE)

$$\frac{\partial \mathbf{q}}{\partial t} = \mathbf{s}. \quad (64)$$

To achieve second order accuracy, and advance the complete solution by Δt , the ODE is first solved with time step $\Delta t/2$. Then the homogeneous equation is solved with time step Δt . Finally, the ODE is again solved with time step $\Delta t/2$. Obviously, at each stage the results from the previous stage are used as initial conditions. This particular operator splitting scheme is known as *Strang splitting*. To solve the ODE equation (64) any standard ODE solution scheme (second order or higher) can be used. In this paper a fourth order Runge–Kutta scheme is used. Another approach is to use the trapezoidal method

$$\mathbf{q}(t + \Delta t) = \mathbf{q}(t) + \frac{1}{2}(\mathbf{s}(\mathbf{q}(t)) + \mathbf{s}(\mathbf{q}(t + \Delta t))). \quad (65)$$

Using a Taylor series expansion for $\mathbf{s}(\mathbf{q}(t + \Delta t))$, after some rearrangements, a semi-implicit update formula for \mathbf{q} is written as

$$\mathbf{q}(t + \Delta t) = \mathbf{q}(t) + \Delta t \left(\mathbf{I} - \frac{\Delta t}{2} \frac{\partial \mathbf{s}}{\partial \mathbf{q}} \right)^{-1} \mathbf{s}(\mathbf{q}(t)). \quad (66)$$

Here $\partial \mathbf{s} / \partial \mathbf{q}$ is the source Jacobian and \mathbf{I} is the unit matrix. Both these ODE solution methods give equally good results and all the simulations presented below use the fourth order Runge–Kutta method. This method makes it simple to add additional source terms without having to compute the source Jacobian.

7. Applications

In the following subsections several example applications of the Two-Fluid algorithms developed in this paper are presented. The applications studied are a one-dimensional Riemann problem, propagation and interaction of solitons in a homogeneous plasma and, collisionless reconnection. Results for these problems obtained with reduced fluid models exist in the literature and hence are used to benchmark the Two-Fluid results. In all cases it is found, as described in detail in the following subsections, the results with the full Two-Fluid model agree (in the appropriate regimes) with those presented in the literature for the simpler models.

As mentioned in Section 1 the high-resolution wave propagation method has been previously applied to other equation systems [5,6,19,20]. In these applications it was shown that with the transverse terms added the scheme is fully second order accurate and allows for Courant numbers upto unity, even for three-dimensional problems. For the Two-Fluid system convergence studies were carried out [7] on electron oscillation problems which confirmed the results of the cited publications.

For all simulations presented below the speed of light is set to $c = 1$, $\epsilon_0 = 1$ and $\gamma = 5/3$.

7.1. Two-Fluid Riemann problem

In many ways the one-dimensional *Riemann problem* defined by

$$\frac{\partial \mathbf{q}}{\partial t} + \frac{\partial \mathbf{f}}{\partial x} = \mathbf{s}, \quad x \in \mathbb{R}, \quad (67)$$

with initial conditions $\mathbf{q}(x < 0, 0) = \mathbf{q}_l$ and $\mathbf{q}(x > 0, 0) = \mathbf{q}_r$, where $\mathbf{q}_{l,r}$ are constant vectors, is fundamental to the solution of hyperbolic balance laws. Solutions to the Riemann problem for the Two-Fluid equations are presented in this section. The Riemann problem selected is a generalization of the Brio–Wu shock-tube problem [22] commonly used to benchmark MHD codes. The initial conditions are

$$\begin{bmatrix} \rho_e \\ u_e \\ v_e \\ w_e \\ p_e \\ \rho_i \\ u_i \\ v_i \\ w_i \\ p_i \\ B_x \\ B_y \\ B_z \\ E_x \\ E_y \\ E_z \end{bmatrix}_l = \begin{bmatrix} 1.0 \frac{m_e}{m_i} \\ 0 \\ 0 \\ 0 \\ 5 \times 10^{-5} \\ 1.0 \\ 0 \\ 0 \\ 0 \\ 5 \times 10^{-5} \\ 0.75 \\ 1.0 \\ 0 \\ 0 \\ 0 \\ 0 \end{bmatrix} \quad \begin{bmatrix} \rho_e \\ u_e \\ v_e \\ w_e \\ p_e \\ \rho_i \\ u_i \\ v_i \\ w_i \\ p_i \\ B_x \\ B_y \\ B_z \\ E_x \\ E_y \\ E_z \end{bmatrix}_r = \begin{bmatrix} 0.125 \frac{m_e}{m_i} \\ 0 \\ 0 \\ 0 \\ 5 \times 10^{-6} \\ 0.125 \\ 0 \\ 0 \\ 0 \\ 5 \times 10^{-6} \\ 0.75 \\ -1.0 \\ 0 \\ 0 \\ 0 \\ 0 \end{bmatrix}, \quad (68)$$

where $m_e/m_i = 1/1832.6$. The only remaining unspecified quantity is the ion charge to mass ratio, $r_i \equiv q_i/m_i$. In terms of this ratio the ion Larmor radius is $r_{Li} \propto 1/r_i$ and the ion-skin depth is $l_i \propto 1/r_i$. Thus it is clear from the discussion of Two-Fluid effects (Eqs. (19) and (20)) that as r_i increases the Larmor radius and skin depth become smaller and the solutions obtained with the Two-Fluid model should approach the solutions obtained with MHD model. Simulations with $q_i/m_i = 1, 10, 100, 1000$ were carried out. These charge to mass ratios correspond to ion-skin depth of 1, 1/10, 1/100, 1/1000, calculated with a reference magnetic field of 1. Thus, for example, for the $q_i/m_i = 1$ simulation the domain length is the same as the ion-skin depth and for the $q_i/m_i = 1000$ the domain length is 1000 times the ion-skin depth. With decreasing ion-skin depth the plasma regime tends toward the ideal MHD limit, as our simulations below confirm. The results are presented for a grid of 50,000 cells. Although the number of grid cells may seem excessive the complex flow physics shown below cannot be resolved on coarser grids, specially with the correct value of the electron–ion mass ratio used.

Fig. 1 shows the mass density computed at $t = 10$ with the ideal MHD model. The solution was computed using an existing shock-capturing non-ideal MHD code [23] by turning off all non-ideal effects. The initial conditions used for the ideal MHD simulation are the same as the standard Brio–Wu shock problem described above. The MHD fluid density was initialized using the ion density and fluid-pressure using total electron and ion pressure. The MHD result serves to compare the solutions obtained with the Two-Fluid model. Comparing the computational time for the ideal-MHD and the full Two-Fluid simulations we found that the Two-Fluid simulations took about 100 times longer. This is not surprising as in the full Two-Fluid system the fastest wave speed is the speed of light which is much larger than the fastest wave speed of the ideal-MHD system (the fast magnetosonic speed).

In Fig. 2 the number densities of electrons and ions are plotted for $q_i/m_i = 1$. This figure shows that for low q/m ratio as the Lorentz force is smaller the fluids can have significant charge separation. In MHD and Hall MHD it is assumed that the electron and ion fluids have the same number densities, i.e. $n_e = n_i$.

Fig. 3 shows the mass density of the ion fluid for $q_i/m_i = 10$. For comparison ideal MHD results are superimposed. Even though the Two-Fluid solution is significantly different from the MHD results the contact discontinuity is in the correct location and the compound wave has started to form. A close-up view of the number densities of the electrons and ions around the compound wave is shown in Fig. 4. It is seen that there

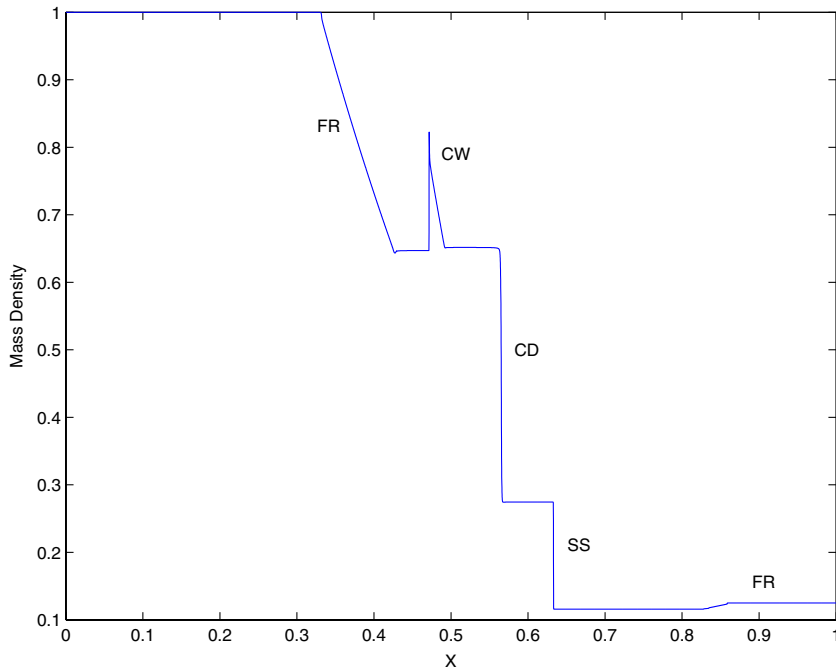


Fig. 1. Fluid mass density at $t = 10$ from an ideal MHD simulation. The various parts of the shock are labeled as follows: contact discontinuity – CD, compound wave – CW, fast rarefaction wave – FR, slow shock – SS.

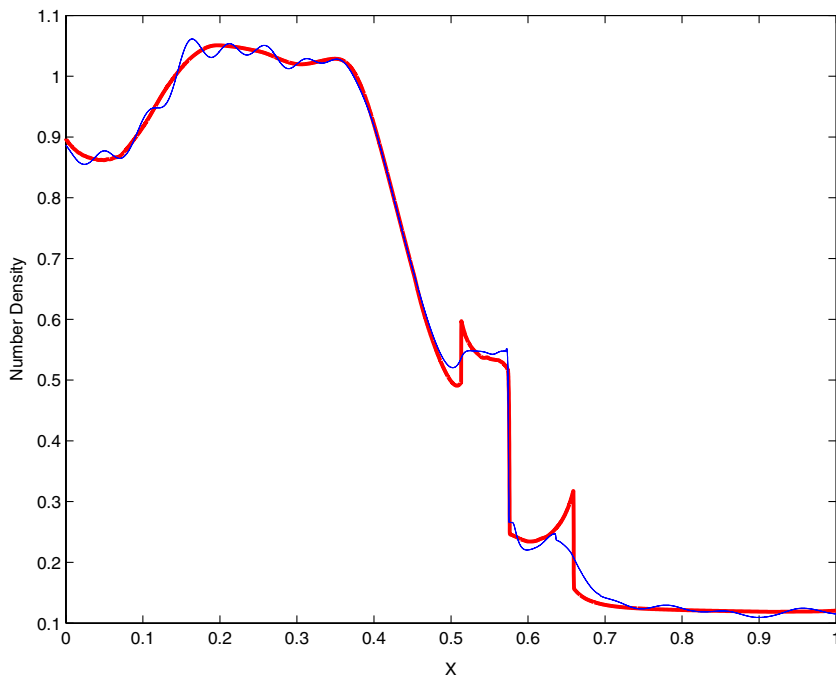


Fig. 2. Electron (light line) and ion (heavy line) number density at $t = 10$ with $q_i/m_i = 1$.

is significant charge separation around the forming compound wave. In general charge separation leads to dispersive waves as is clearly visible in this plot. Dispersive effects due to charge separation play an important role in the formation of ion-acoustic solitons as discussed in a later section.

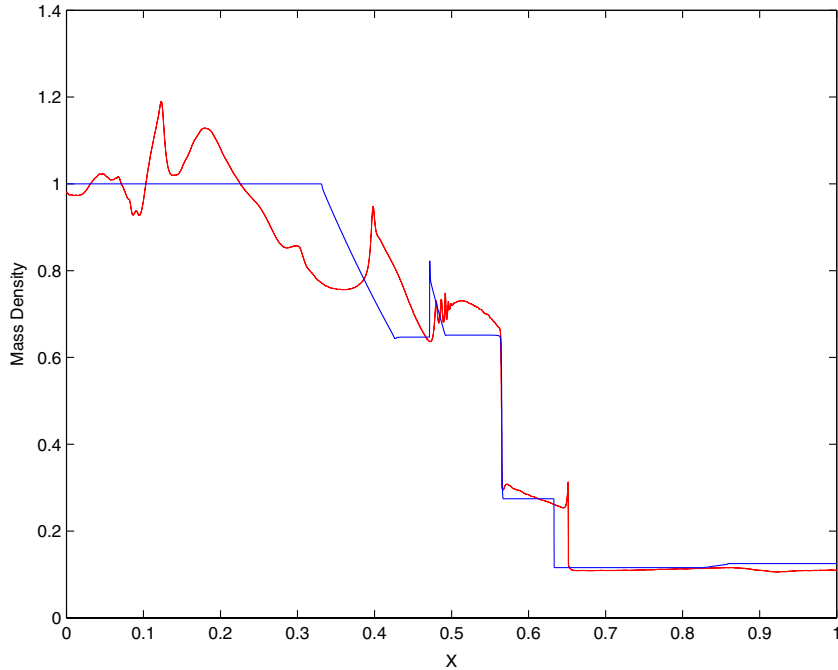


Fig. 3. Ion mass density (red line) at $t = 10$ with $q_i/m_i = 10$. Also plotted is the ideal MHD mass density (blue line). The Two-Fluid solution shows the compound wave and slow shock developing while the contact discontinuity is at the correct location. (For interpretation of the references to color in this figure legend, the reader is referred to the web version of this article.)

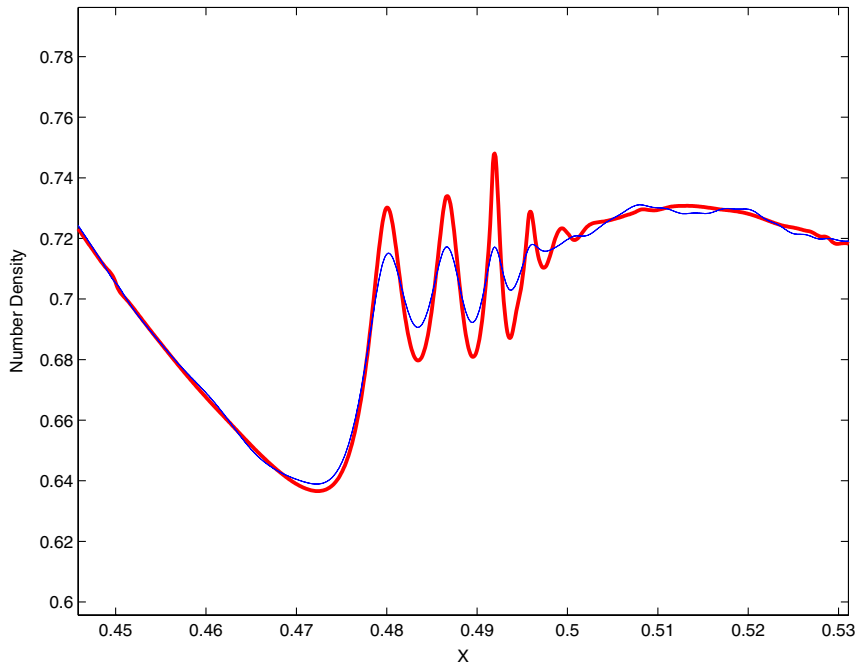


Fig. 4. Ion (heavy line) and electron (light line) number densities at $t = 10$ with $q_i/m_i = 10$ around the compound wave. The dispersive waves are formed due to charge separation effects.

Fig. 5 shows the mass density of the ion fluid for $q_i/m_i = 1000$. The Two-Fluid solutions are now clearly MHD like: the compound wave has now formed and fast rarefaction waves (upstream and downstream) and contact discontinuity are all in the correct locations. The slow shock, however, seems to be moving slower

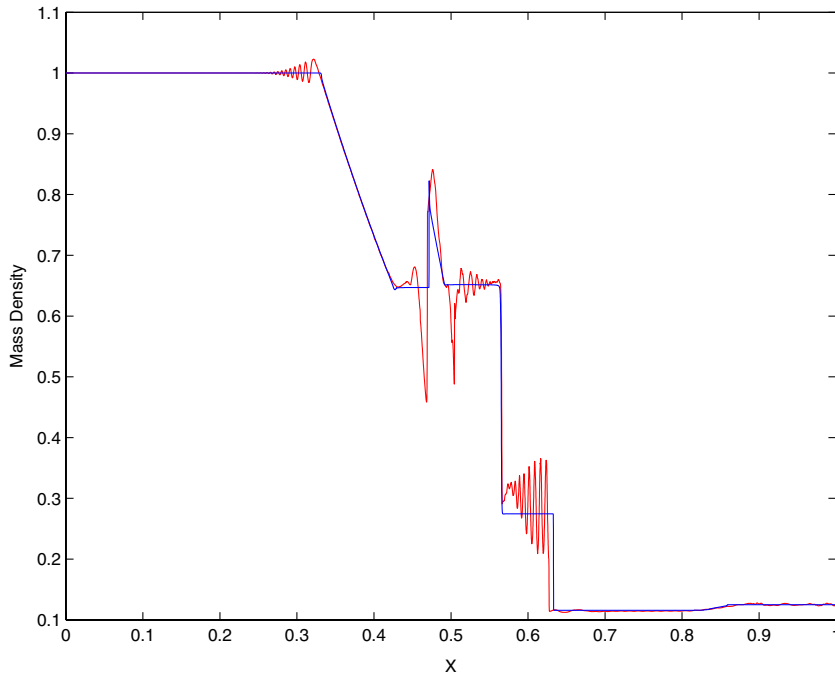


Fig. 5. Ion mass density (red line) at $t = 10$ with $q_i/m_i = 1000$. Also plotted is the ideal MHD mass density (blue line). The compound wave has now formed in the Two-Fluid solution. The fast rarefaction waves (upstream and downstream) and contact discontinuity are all in the correct locations. The slow shock, however, seems to be moving slower than in the MHD solution. (For interpretation of the references to color in this figure legend, the reader is referred to the web version of this article.)

than the MHD result. A close-up of the solutions is shown in Fig. 6. Dispersive waves are clearly seen and these are conjectured to be dispersive magnetosonic waves, as evidenced from dispersion relations computed and presented as Fig. 11 in [7].

In conclusion, the Two-Fluid Riemann problem serves not only as an important benchmark for the algorithms, but also highlights the complex Two-Fluid physics not captured in the simpler MHD model.

7.2. Soliton propagation

Soliton propagation in fluids and plasmas is an active area of research [24–26]. Much previous work has been done in plasma physics on soliton propagation in the weakly nonlinear limit. In this limit, using expansion techniques, the Korteweg–de Vries (KdV) equation can be derived and either solved numerically or a particular class of solutions studied analytically. An example of this approach is the study of ion-acoustic solitons [8] in which the electrons are assumed to be a massless isothermal fluid and the ions are assumed cold (i.e. the ion pressure vanishes). With these assumptions a KdV equation can be derived which describes the propagation of soliton structures in the ion fluid. An important outcome of this analysis is that the dispersive effects needed to support soliton formation arise from non-neutral (charge-separation) effects. Thus ion-acoustic solitons cannot be simulated using fluid models which assume quasi-neutrality, like the MHD and Hall MHD models.

In this section simulations are carried out to show that ion-acoustic solitons can form from an initial density hump or “slug”. These solutions are in the strongly nonlinear regime and hence cannot be described with a standard KdV equation. Similar structures have been observed experimentally [27]. Numerical simulations of density slug induced solitons were carried out by Baboolal [24] who assumed an isothermal electron fluid and an adiabatic ion fluid with adiabatic index $\gamma = 3$. With these assumptions there is no need to solve an energy equation as the equation of state $p\rho^{-\gamma} = \text{constant}$ is used to calculate the pressure. In the simulation performed here these assumptions are not made. It is shown that a stable stationary structure, not observed in



Fig. 6. Close up of ion mass density (red line) around the slow shock at $t = 10$ with $q_i/m_i = 1000$. Also plotted is the ideal MHD mass density (blue line). The ion density oscillations are due to dispersive magnetosonic waves. (For interpretation of the references to color in this figure legend, the reader is referred to the web version of this article.)

the simulations of Babooyal, arises in addition to the traveling solitons. Such stationary density structures cannot be supported in adiabatic fluids as a density gradient implies a pressure gradient which in turn implies flow.

The plasma is assumed to be stationary, i.e. $\mathbf{u}_e(x, t = 0) = \mathbf{u}_i(x, t = 0) = \mathbf{0}$. The electron and ion number densities are initialized as $n_e = n_i = n(x)$ where

$$n(x) = 1 + \exp\left(-\frac{1}{2}|x - x_c|\right), \quad (69)$$

where $x \in [0, L_x]$ and $x_c = L_x/4$. The ion–electron temperature ratio (where temperature, T , is computed from the relation $p = nT$) is set to 1/100. The initial pressure profile is set using $p_\alpha(x, t = 0) = n_\alpha T_\alpha$ for $\alpha \in \{e, i\}$. The domain size is $L_x = 12c/\omega_{pi}$ calculate using $n_i = 1$ and $q_i/m_i = 1$, and is discretized using 1500 cells. The electron–ion mass ratio is $m_e/m_i = 1/25$. The boundary conditions are periodic. The value x_c and boundary conditions were selected to ensure that solitons leaving the domain from one side would reappear from the opposite side and soliton interaction would occur inside the domain and not on the boundaries.

Figs. 7 and 8 show the time evolution of the ion density. It is seen that two solitons emerge from the initial slug and travel in opposite directions. The soliton speed is calculated and is approximately $1.01 c_{si}$, where c_{si} is the ion fluid sound speed. This value agrees well with a linear analysis of ion-acoustic solitons. A trail of decaying plasma waves is also seen in the soliton wake. This feature is common to solitons generated in dispersive systems. As the boundary conditions are periodic the solitons reenter the domain and collide at $x = 10$. After collision the solitons reemerge with their shapes unchanged. Later in time the solitons merge with the stationary structure at $x = 4$ approximately recreating the initial conditions. The stationary structure is seen to be stable to interactions. For the grid (1500 cells) used the solitons cross the domain about 40 times before becoming significantly damped out. For a coarser grid the solitons damp out faster due to the grid diffusion.

The results obtained here compare well with those obtained by Babooyal. However in Babooyal's [24] simulations the central stationary structure does not form due to the selected equation of state. In the simulations performed here the pressure is constant across the stationary structure and hence the density there remains constant in time.

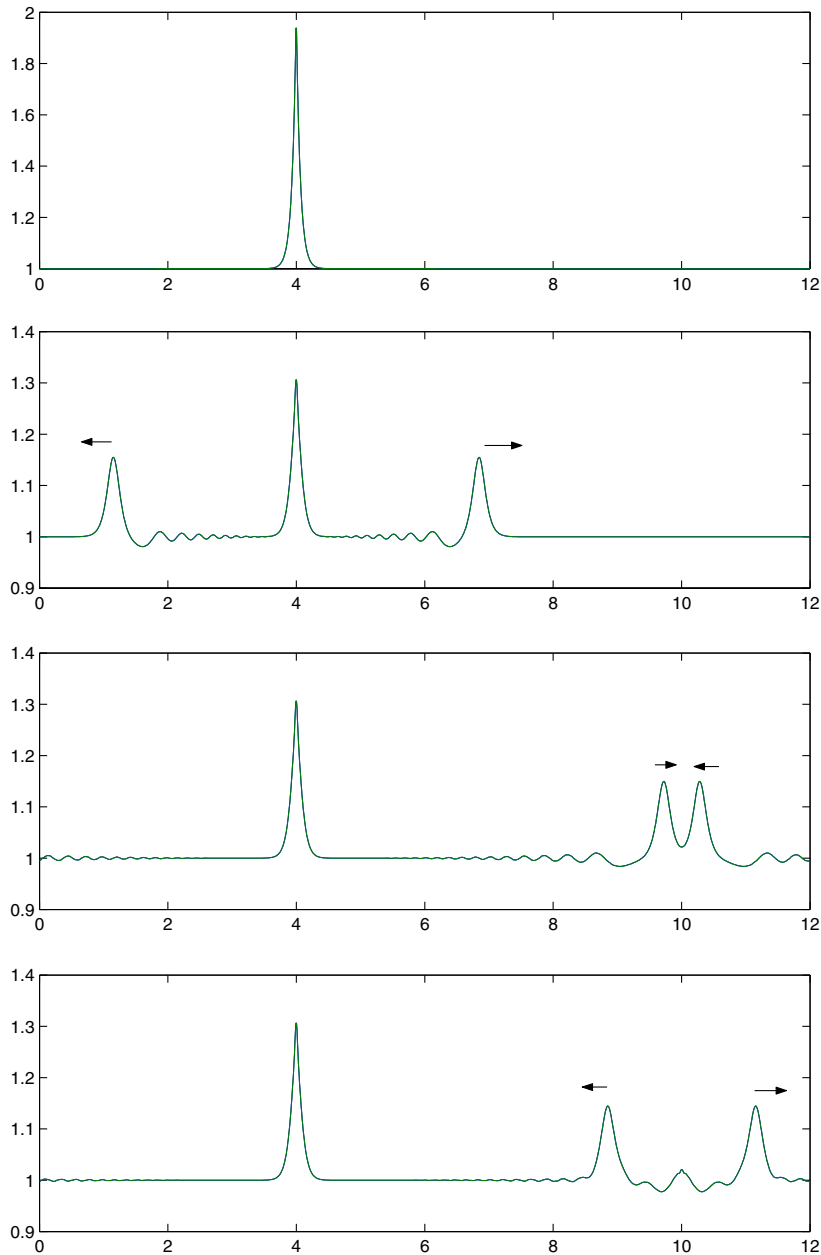


Fig. 7. Ion mass density for soliton propagation and interaction. The frames correspond to, from top to bottom, $t = 0, 100, 200, 250$, measured in inverse ion-cyclotron frequency. The arrows show direction of propagation of the solitons. Solitons collide and reemerge without change in shape.

7.3. Collisionless reconnection

Magnetic reconnection [28] is the process by which the topology of the magnetic field lines changes. In ideal MHD or ideal Hall MHD the field line topology cannot change and this is described by saying that field lines are “frozen” into the fluid (frozen into the electron fluid in case of ideal Hall-MHD). The situation is analogous to neutral ideal fluid flow in which vortex tube topology remains constant. However even small resistivity (viscosity in neutral fluids) can make the topology change and the field lines reconnect and this process is adequately described in the framework of resistive MHD or Hall-MHD.

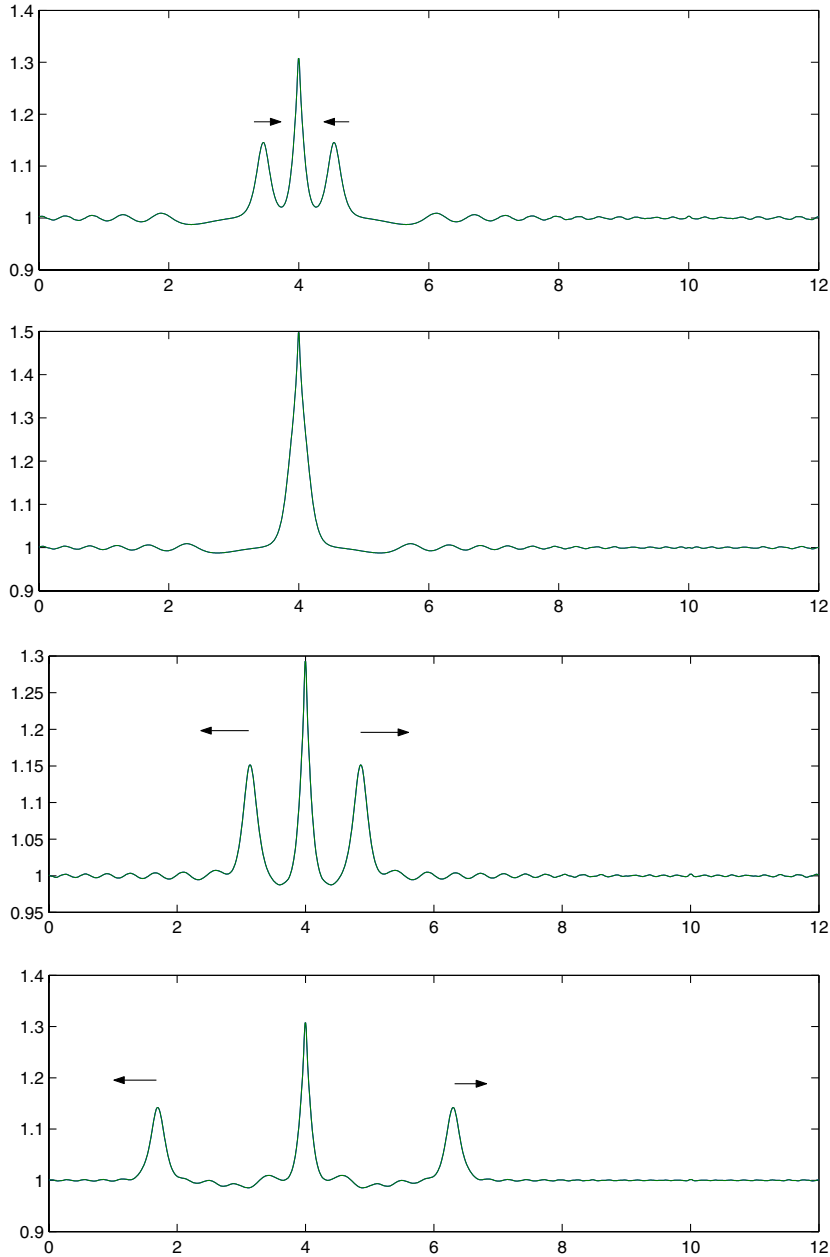


Fig. 8. Ion mass density for soliton propagation and interaction. The frames correspond to, from top to bottom, $t = 400, 415, 450, 500$, measured in inverse ion-cyclotron frequency. The arrows show direction of propagation of the solitons. The two solitons combine with the central stationary structure to approximately recreate the initial conditions. The central structure is stable to interactions.

However, in a collisionless plasma magnetic reconnection is also observed to occur and at a much faster rate than in collisional plasmas. This *fast collisionless reconnection* is important in understanding many space plasma phenomena, for example, solar flares and the dynamics of the Earth's magnetotail during a geomagnetic substorm. To understand the mechanism of collisionless reconnection a number of plasma models were used to study collisionless reconnection of oppositely directed magnetic fields separated by a thin current sheet. This effort went under the rubric of geospace environmental modeling (GEM) reconnection challenge [29]. The various models used were electron MHD [30], Hall MHD with anisotropic pressure [31], MHD and Hall MHD [32–34], full particle [35] and hybrid [36] models. It was found that the although reconnection

initiates at length scales on the order of the electron skin depth the reconnection rate is governed by ion dynamics. The Two-Fluid model can describe the physics at electron-skin depth scales and hence can describe collisionless reconnection correctly. On the electron-skin depth scales the field lines are no longer frozen to the electron fluid and this allows the reconnection to initiate without the need for resistivity. On the other hand in the Hall MHD model [34] the reconnection needs to be initiated by using a small resistivity.

In this section simulations are performed with the same initial conditions and parameters as used in the GEM challenge problem. The ideal Two-Fluid model used here was not among one of those used in the original studies and hence serves as an important benchmark. The results obtained here also provide additional insight into the structure of the flow, specially after the reconnection has occurred. As is described below, complex flows, not observed in the results reported in the original studies, are obtained.

The simulation is initialized with oppositely directed magnetic fields separated by a thin current sheet. The magnetic field is given by

$$\mathbf{B}(y) = B_0 \tanh(y/\lambda) \mathbf{e}_x. \quad (70)$$

The initial current is carried only by the electrons:

$$\mathbf{J}_e = -\frac{B_0}{\lambda} \operatorname{sech}^2(y/\lambda). \quad (71)$$

The number densities of the ions and electrons are initialized as $n_e(y) = n_i(y) = n(y)$, where

$$n(y) = n_0(1/5 + \operatorname{sech}^2(y/\lambda)). \quad (72)$$

Finally, the electron pressure is set to $p_e(y) = p(y)$ and ion pressure to $p_i(y) = 5p(y)$ where

$$p(y) = \frac{B_0}{12} n(y). \quad (73)$$

These initial conditions describe an equilibrium solution of the Two-Fluid equations. To initiate reconnection in a controlled manner the magnetic field is perturbed with $\delta\mathbf{B} = \mathbf{e}_z \times \nabla\psi$, where

$$\psi(x, y) = \psi_0 \cos(2\pi x/L_x) \cos(\pi y/L_y), \quad (74)$$

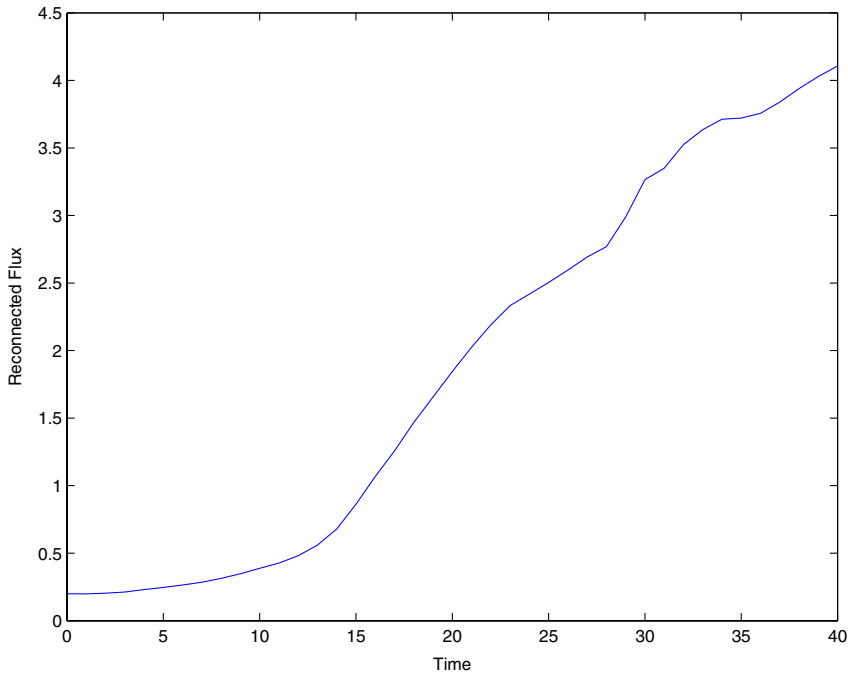


Fig. 9. Reconnected flux versus time. The reconnected flux increases rapidly after the reconnection occurs at about $t = 10$.

and $[-L_x/2, L_x/2] \times [-L_y/2, L_y/2]$ is the simulation domain. This form of the perturbation assures that $\nabla \cdot \mathbf{B} = 0$ at $t = 0$. Periodic boundaries are applied at $x = \pm L_x/2$ and conducting wall boundaries at $y = \pm L_y/2$. Simulations presented below are for a 512×256 grid, although coarser grids were also used. The other parameters used are $m_e/m_i = 1/25$, $L_x = 8\pi$, $L_y = 4\pi$, $B_0 = 0.1$, $\psi_0 = B_0/10$ and $\lambda = 0.5$. The unit length scale is the ion-skin depth and the unit time scale is in inverse ion cyclotron frequency. For the selected electron–ion mass ratio the electron-skin depth is $1/5$ and is resolved by the grid. These parameters are identical with the GEM challenge problem.

To compare results with the models used in the GEM challenge problem the reconnected flux, ϕ , was computed using

$$\phi(t) = \frac{1}{2L_x} \int_{-L_x/2}^{L_x/2} |B_y(x, y = 0, t)| dx. \quad (75)$$

As the reconnection proceeds the reconnected flux, which is a measure of the net Y direction magnetic field, increases and indicates the reconnection rate. Fig. 9 shows the reconnected flux history. It is observed that the reconnection occurs at about $t = 10$ and the reconnected flux increases rapidly after that. The computed

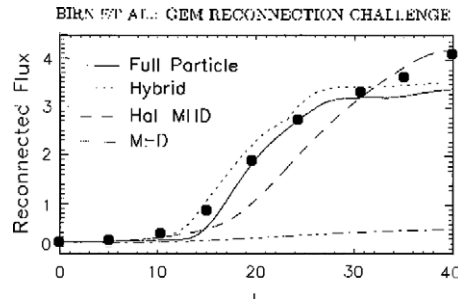


Fig. 10. Two-Fluid reconnected flux compared to GEM results. Solid dots are results obtained using Two-Fluid model. Two-Fluid results compare well with those obtained by particle and hybrid models.

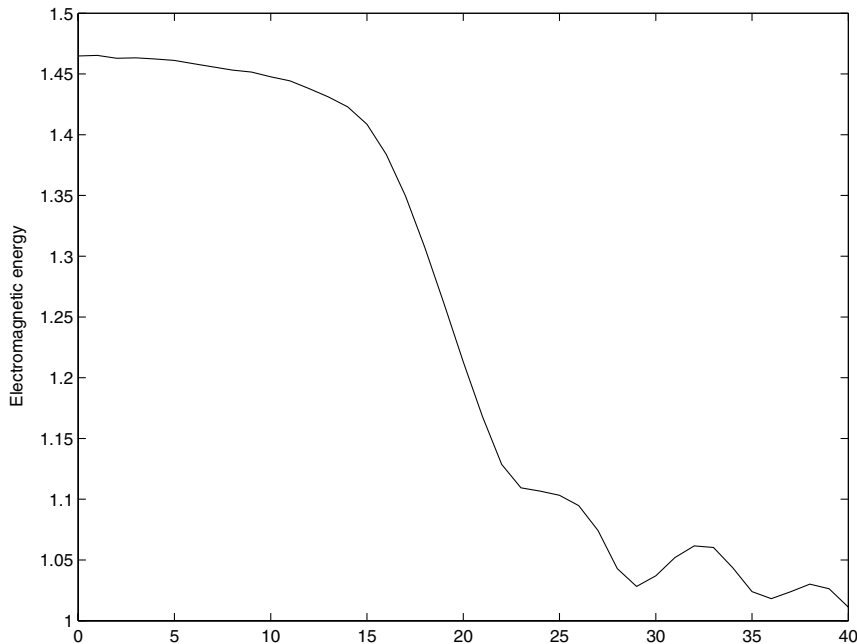


Fig. 11. Electromagnetic energy as a function of time. After reconnection occurs the electromagnetic energy decays, the released energy being transferred to fluid thermal and kinetic energies.

flux history is in excellent agreement with flux histories from full particle and hybrid models used in the original GEM challenge problem (see Fig. 10). From the GEM results it is also clear that the resistive Hall-MHD model also predicts the correct reconnected flux. However, in contrast to resistive Hall-MHD the Two-Fluid model

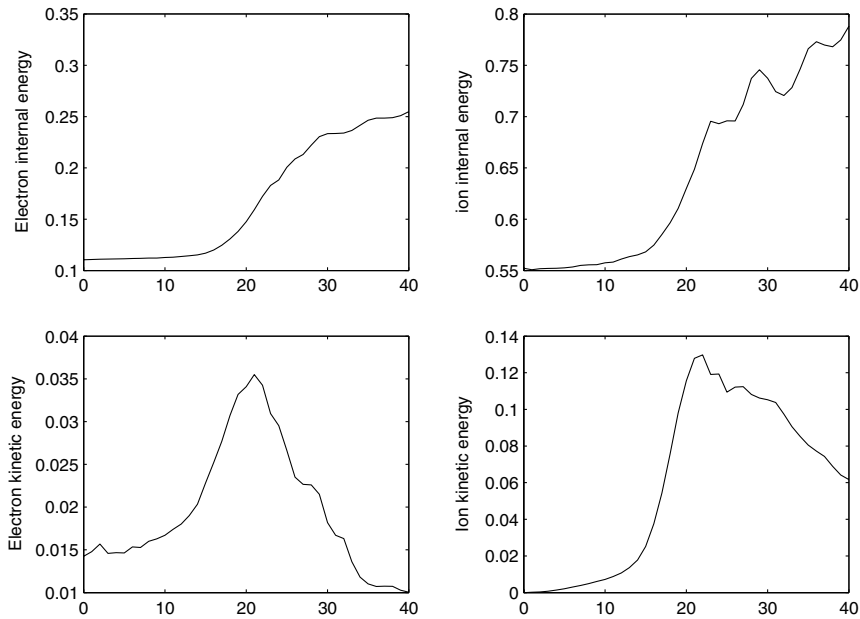


Fig. 12. Electron thermal energy (top left), ion thermal energy (top right), electron kinetic energy (bottom left) and ion kinetic energy (bottom right). The electromagnetic energy released is transformed into kinetic and thermal energy of the fluids. After about $t = 25$ fluid kinetic energies decay as fluids become turbulent.

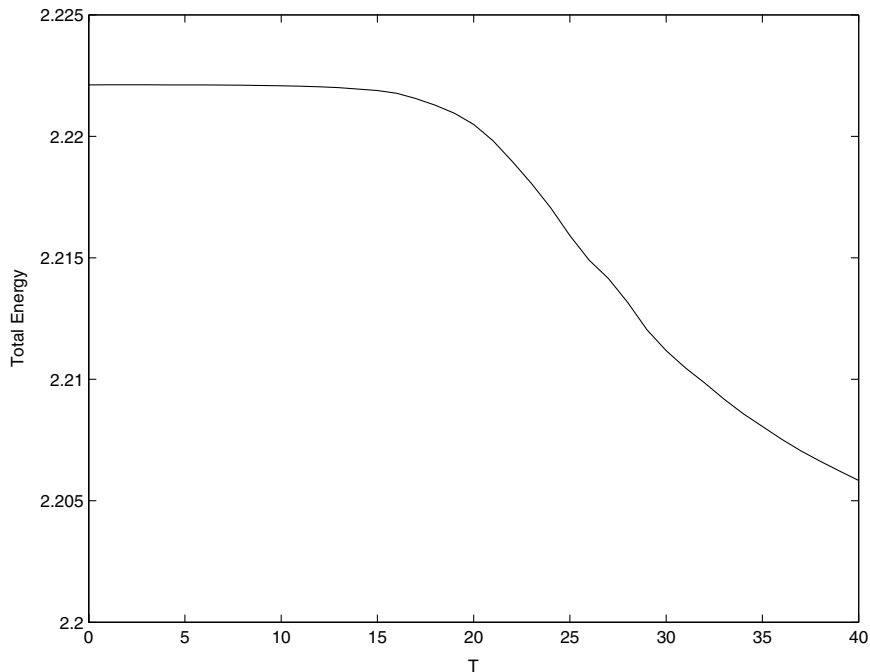


Fig. 13. Total energy for the GEM magnetic reconnection challenge problem. The total energy should remain conserved, however, is seen to decay slightly due to numerical diffusion. The total loss in energy is 0.7% for the time period considered.

presented here does not have any resistivity. The reconnection initiates due to the demagnetization of the electrons at electron-skin depth scales, and thus resistivity is not required to break the field lines as in Hall-MHD. Thus, in the Two-Fluid model the magnetic field-line topology is not tied to the electron fluid as it is in the ideal Hall-MHD.

As the domain is periodic in the Y direction and there are conducting walls on the $x = \pm L_y/2$ the total energy of the system remains constant in time. Figs. 11 and 12 show the history of the electromagnetic and fluid energies of the system. The initial configuration of the system is an unstable equilibrium and via the process of reconnection the magnetic field “relaxes”, i.e. the electromagnetic energy stored in the magnetic field is transferred to the fluid energy. The electromagnetic energy decays rapidly after about $t = 10$ and is transferred to the fluid energy. After $t = 25$ the fluid kinetic energy decreases and is transferred to the fluid thermal energy. Even though the fluids are inviscid this conversion occurs due to adiabatic compression of the fluid. Further, the fluid undergoes shock-heating as the shock waves, visible in Figs. 14 and 15, pass through the fluid.

Fig. 13 shows the total energy of the system. The total energy should be conserved as the Two-Fluid system does not have any dissipation and conducting wall boundary conditions are used. However, due to numerical diffusion the total energy reduces slightly. From the figure it is clear that the loss in energy is only about 0.7%, showing that the scheme used here is conservative even in the presence of complex flow features.

Electron and ion momentum at $t = 25$ and $t = 40$ are shown in the gray-scale plots, Figs. 14 and 15. At $t = 25$ shocks waves traveling inwards (towards the Y axis) are observed. These shocks are formed due to

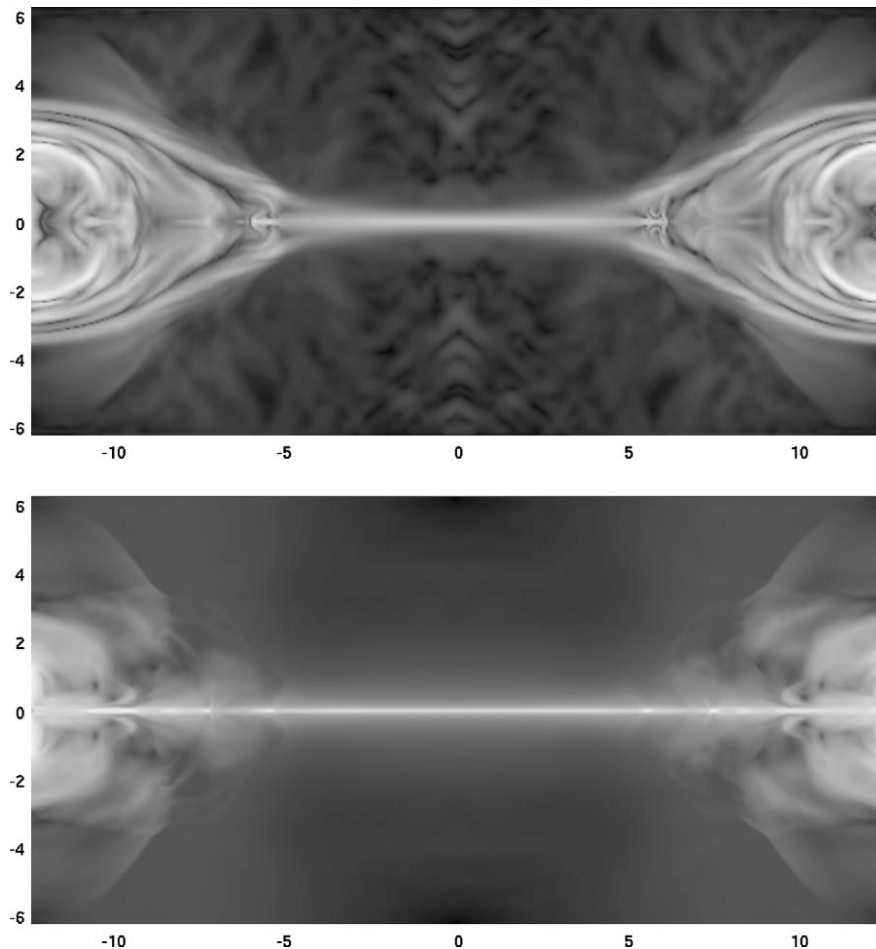


Fig. 14. Electron momentum (top) and ion momentum (bottom) at $t = 25$. Inward traveling shock waves are visible in both the fluids. Thin jets flowing along the X axis are also visible.

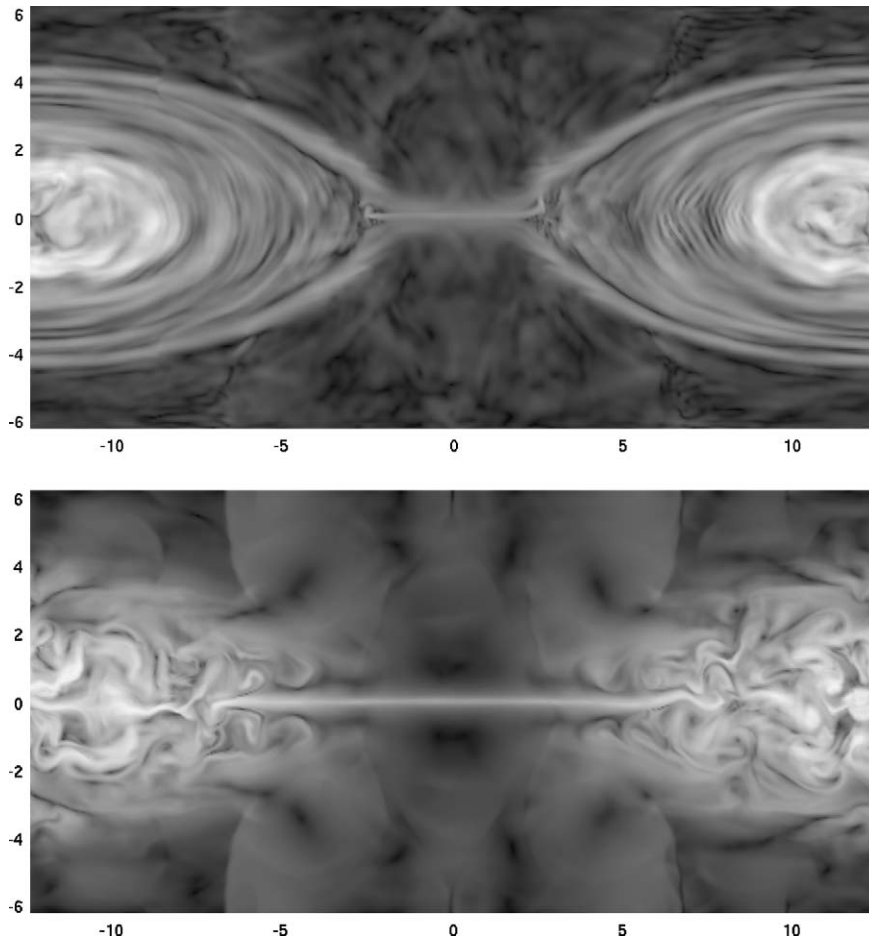


Fig. 15. Electron momentum (top) and ion momentum (bottom) at $t = 40$. Complex flow features are visible, specially in the ion fluid. Flow structure is thought to develop due to instabilities.

the interaction of the outward flowing jets (along the X axis). At $t = 40$ complex flow structures are seen in the ion fluid. The shocks at $x \approx \pm 5.5$ are now moving outwards (away from the Y axis). The ion flow is not symmetric and this may be due to grid driven instabilities. The nature of the flow at late times seems to be governed by instabilities driven from the counter streaming fluid jets.

8. Conclusion

A high resolution wave propagation scheme for ideal Two-Fluid Plasma equations is developed. The algorithm presented here can be successfully used to in multiple dimensions. The algorithm can also be extended to general quadrilateral geometries easily. An important aspect of this work was to highlight Two-Fluid physics which is not included in the commonly used MHD and Hall MHD models. The three applications presented here each show the importance of Two-Fluid physics. In the one-dimensional Riemann problem it was shown that a smooth transition from neutral ideal fluid shocks to MHD shocks can be obtained. The ion-acoustic soliton propagation showed the importance of charge separation. In fact, the dispersive effects due to charge separation balance the tendency of the fluid to shock and hence lead to soliton propagation. In both MHD as well as Hall MHD ion-acoustic solitons cannot be supported as quasi-neutrality ($n_e = n_i$) is assumed. The GEM reconnection challenge problem showed that the Two-Fluid model can correctly explain fast reconnection observed in collisionless plasmas. In other fluid models of reconnection some mechanism (like resistivity in Hall MHD) needs to be incorporated to initiate the reconnection. Complex flows, possibly turbulent, can be

seen late after the reconnection has occurred. The algorithm presented here can also be applied directly to higher-moment fluid approximation to collisionless plasmas. For example, the next two set of collisionless fluid equations contain, for s species plasma, $10s$ and $20s$ fluid equations. These higher-moment equations incorporate anisotropic pressure and heat tensor effects and hence extend the usefulness of fluid plasma models.

Non-ideal effects like resistivity and radiation can also be added to the basic algorithm presented here. In this case the equation system is no longer hyperbolic but has parabolic parts from the non-ideal terms. Although the high-resolution wave propagation scheme is designed for hyperbolic equations these non-ideal terms can be incorporated as source terms, which now contain second or higher-order derivatives. Such an approach has been discussed by LeVeque [5] for the diffusive Burgers equation. Including non-ideal terms will also effect the results presented here. For example, it is known that gyroviscous stress-tensor can anisotropically heat the ions near the reconnection point during magnetic reconnection. However, this should not change the reconnected flux significantly. The focus of this paper being the ideal full Two-Fluid model we have ignored all non-ideal effects for the results presented.

Acknowledgments

The authors acknowledge computer time on the Ladon Supercomputer belonging to the Mechanical Engineering Department of the University of Washington, Seattle. Helpful comments from the reviewers is also acknowledged.

References

- [1] L. Woods, *Physics of Plasmas*, Wiley-VCH, New York, 2004.
- [2] J.P. Friedberg, *Ideal Magnetohydrodynamics*, Plenum Press, New York, 1987.
- [3] J. Loverich, A. Hakim, U. Shumlak, A discontinuous Galerkin method for ideal two-fluid plasma equations, *Journal of Computational Physics*, submitted for publication.
- [4] C.-D. Munz, P. Omnes, R. Schneider, E. Sonnendrücker, U. Voß, Divergence correction techniques for Maxwell solvers based on a hyperbolic model, *Journal of Computational Physics* 161 (2000) 484–511.
- [5] R.J. LeVeque, *Finite Volume Methods For Hyperbolic Problems*, Cambridge University Press, Cambridge, 2002.
- [6] J. Rossmannith, A wave propagation method with constrained transport for ideal and shallow water magnetohydrodynamics, Ph.D. Thesis, University of Washington, 2002.
- [7] U. Shumlak, J. Loverich, Approximate Riemann solver for the two fluid plasma model, *Journal of Computational Physics* 187 (2003) 620–638.
- [8] R.C. Davidson, *Methods in Nonlinear Plasma Theory*, Academic Press, New York, 1972.
- [9] A. Ishimaru, *Electromagnetic Wave Propagation, Radiation and Scattering*, Prentice-Hall, Englewood Cliffs, NJ, 1991.
- [10] L. Steinhauer, A. Ishida, Relaxation of two-species magnetofluid and application to finite- β flowing plasma, *Physics of Plasmas* 5 (7) (1998) 2609–2622.
- [11] J. Büchner, C. Dunn, M. Scholer (Eds.), *Space Plasma Simulations*, Springer, New York, 2003.
- [12] L.C. Steinhauer, H. Yamada, A. Ishida, Two-fluid flowing equilibria of compact plasmas, *Physics of Plasmas* 8 (9) (2001) 4053–4061.
- [13] R. Davidson, N. Gladd, Anomalous transport properties associated with the lower-hybrid-drift instability, *The Physics of Fluids* 18 (10) (1975) 1327–1335.
- [14] J. Huba, N. Gladd, Lower-hybrid-drift instability in field reversed plasmas, *Physics of Fluids* 23 (3) (1980) 552–561.
- [15] B.-N. Jiang, J. Wu, L. Povinelli, The origin of spurious solutions in computational electromagnetics, *Journal of Computational Physics* 125 (1996) 104–123.
- [16] C.-D. Munz, P. Omnes, R. Schneider, A three-dimensional finite-volume solver for the Maxwell equations with divergence cleaning on unstructured meshes, *Computer Physics Communications*.
- [17] C.-D. Munz, U. Voß, A finite-volume method for the Maxwell equations in the time domain, *SIAM Journal of Scientific Computing* 22 (2) (2000) 449–475.
- [18] A.G. Kulikovskii, N.V. Pogorelov, A.Y. Semenov, *Mathematical Aspects of Numerical Solutions of Hyperbolic Systems*, Chapman & Hall/CRC, London/Boca Raton, FL, 2001.
- [19] D. Bale, R.J. LeVeque, S. Mitran, J.A. Rossmannith, A wave-propagation method for conservation laws and balance laws with spatially varying flux functions, *SIAM Journal of Scientific Computing* 24 (2002) 955–978.
- [20] J.O. Langseth, R. LeVeque, A wave propagation method for three-dimensional hyperbolic conservation laws, *Journal of Computational Physics* 165 (2000) 126–166.
- [21] P. Roe, Approximate Riemann solvers, parameter vectors, and difference schemes, *Journal of Computational Physics* 43 (1981) 357–372.

- [22] M. Brio, C. Wu, An upwind differencing scheme for the equations of ideal magnetohydrodynamics, *Journal of Computational Physics* 75 (1988) 400–422.
- [23] O.S. Jones, U. Shumlak, D.S. Eberhardt, An implicit scheme for nonideal magnetohydrodynamics, *Journal of Computational Physics* 130 (1997) 231–242.
- [24] S. Baboolal, Finite-difference modeling of solitons induced by a density hump in a plasma multi-fluid, *Mathematics and Computers in Simulation* 55 (2001) 309–316.
- [25] J. McKenzie, T. Doyle, Oblique solitons in a cold magnetized plasma, *Physics of Plasmas* 8 (10) (2001) 4367–4374.
- [26] J. McKenzie, T. Doyle, The properties of fast and slow oblique solitons in a magnetized plasma, *Physics of Plasmas* 9 (1) (2001) 55–63.
- [27] D. Cohn, K. McKenzie, Density-step-excited ion-acoustic solitons, *Physical Review Letters* 30 (1973) 258–261.
- [28] E. Priest, T. Forbes, *Magnetic Reconnection*, Cambridge University Press, Cambridge, 2000.
- [29] J. Birn et al., Geospace environment modeling (GEM) magnetic reconnection challenge, *Journal of Geophysical Research* 106 (2001) 3715.
- [30] M. Hesse, J. Birn, M. Kuznetsova, Collisionless magnetic reconnection: electron processes and transport modeling, *Journal of Geophysical Research* 106 (A3) (2001) 3721.
- [31] J. Birn, M. Hesse, Geospace environment modeling (GEM) magnetic reconnection challenge: resistive tearing, anisotropic pressure and Hall effects, *Journal of Geophysical Research* 106 (A3) (2001) 3737.
- [32] A. Otto, Geospace environment modeling (GEM) magnetic reconnection challenge: MHD and Hall MHD – constant and current dependent resistivity models, *Journal of Geophysical Research*.
- [33] M. Shay, J. Drake, B. Rogers, R. Denton, Alfvénic collisionless magnetic reconnection and the Hall term, *Journal of Geophysical Research*.
- [34] Z. Ma, A. Bhattacharjee, Hall magnetohydrodynamic reconnection: the geospace environment modeling challenge, *Journal of Geophysical Research* 106 (A3) (2001) 3773.
- [35] P. Prichette, Geospace environment modeling magnetic reconnection challenge: simulations with a full particle electromagnetic code, *Journal of Geophysical Research* 106 (A3) (2001) 3783.
- [36] M.M. Kuznetsova, M. Hesse, D. Winske, Collisionless reconnection supported by nongyrotropic pressure effects in hybrid and particle simulations, *Journal of Geophysical Research* 106 (A3) (2001) 3799.